Functional evaluation of the P681H mutation on the proteolytic activation the SARS-CoV-2 variant B.1.1.7 (Alpha) spike

Bailey Lubinski [1], Maureen H. V. Fernandes [2], Laura Frazier [1], Tiffany Tang [3], Susan Daniel [3], Diego G. Diel [2], Javier A. Jaimes [1*] and Gary R. Whittaker [1,4*]

[1] Department of Microbiology & Immunology, College of Veterinary Medicine, Cornell University, Ithaca, NY, 14853, USA.

[2] Department of Population Medicine, College of Veterinary Medicine, Cornell University, Ithaca, NY, 14853, USA.

[3] Robert Frederick Smith School of Chemical & Biomolecular Engineering, Cornell University, Ithaca, NY, 14853, USA.

[4] Master of Public Health Program, Cornell University, Ithaca, NY, 14853, USA.

*Corresponding authors

618 Tower Rd., Ithaca NY 14853, USA

jaj246@cornell.edu; grw7@cornell.edu

Highlights:

- SARS-CoV-2 B.1.1.7 VOC has a P681H mutation in the spike that is predicted to enhance viral infection
- P681H does not significantly impact furin cleavage, viral entry or cell-cell spread
- Other mutations in the SARS-CoV-2 B.1.1.7 VOC may account for increased infection rates

24 **Graphical abstract:**

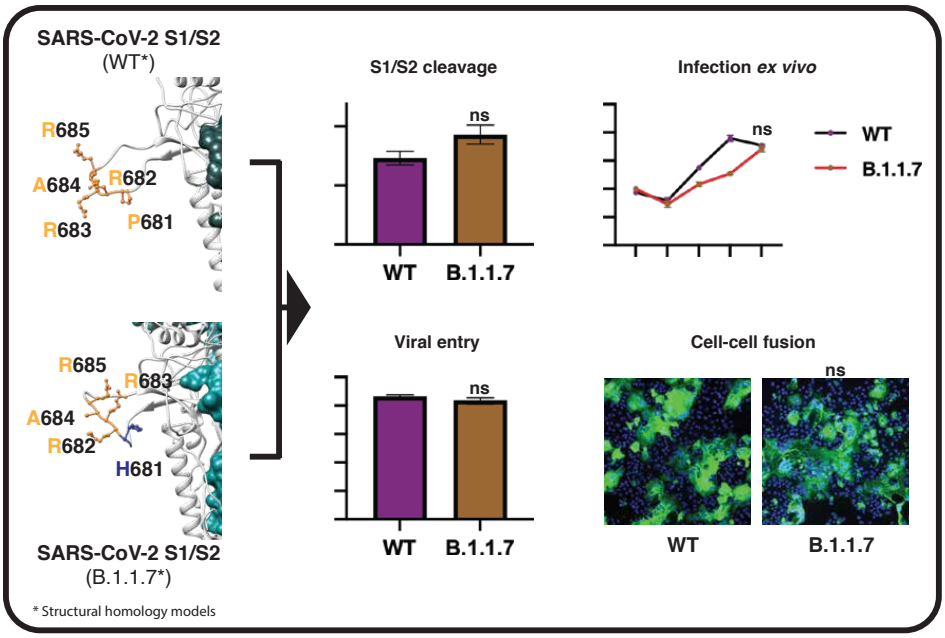

25

26

27 **Summary**

28 Severe acute respiratory syndrome coronavirus 2 (SARS-CoV-2) is the agent causing the COVID-19
29 pandemic. SARS-CoV-2 B.1.1.7 (Alpha), a WHO variant of concern (VOC) first identified in the UK
30 in late 2020, contains several mutations including P681H in the spike S1/S2 cleavage site, which is
31 predicted to increase cleavage by furin, potentially impacting the viral cell entry. Here, we studied the
32 role of the P681H mutation in B.1.1.7 cell entry. We performed assays using fluorogenic peptides
33 mimicking the Wuhan-Hu-1 and B.1.1.7 S1/S2 sequence and observed no significant difference in
34 furin cleavage. Functional assays using pseudoparticles harboring SARS-CoV-2 spikes and cell-to-cell
35 fusion assays demonstrated no differences between Wuhan-Hu-1, B.1.1.7 or a P681H point mutant.
36 Likewise, we observed no differences in viral growth between USA-WA1/2020 and a B.1.1.7 isolate
37 in cell culture. Our findings suggest that while the B.1.1.7 P681H mutation may slightly increase S1/S2
38 cleavage this does not significantly impact viral entry or cell-cell spread.

39

40 **Introduction**

41 Severe acute respiratory syndrome coronavirus 2 (SARS-CoV-2) is the agent behind the current
42 COVID-19 pandemic (Whittaker et al., 2021). SARS-CoV-2 emerged from a yet to be determined
43 animal reservoir and was first identified in late 2019; it has since rapidly spread throughout the world.
44 The virus now exists in two lineages, A and B. While both lineages remain in circulation globally, the
45 B lineage became the dominant virus following its introduction into Northern Italy in February 2020.
46 The B lineage has undergone significant diversification as it expanded, and in particular acquired an S
47 gene mutation (D614G) that resulted in a more stabilized spike protein, which has been linked to
48 increased transmissibility (Zhou et al., 2021). D614G has now become established in circulating B
49 lineage viruses.

50 In late summer to early fall 2020, a new variant of SARS-CoV-2 was identified in the UK, based on S-
51 gene target failures in community-based diagnostic PCR testing (Rambaut et al., 2020). Following
52 subsequent sequence analysis, this variant was defined as variant of concern (VOC) B.1.1.7/501Y.V1
53 by Public Health England, and later denominated as the Alpha variant. B.1.1.7 rapidly expanded across
54 the south of England and subsequently spread to other parts of the U.K. (Volz et al., 2021), and then
55 globally. The B.1.1.7 VOC was unusual compared to other SARS-CoV-2 variants emerging at that
56 time in that is contained a higher than typical level of point mutants across its genome; 23 in total. Of
57 particular note were nine mutations in the spike gene compared to prototype sequences; a 69-70
58 deletion, Y144 del, N501Y, A570D, D614G, P681H, T716I, S982A, and D118H, with seven of these
59 distinct to B.1.1.7. One of the more concerning mutations was N501Y, which was linked (along with
60 D614G) to increased affinity of the spike protein to the SARS-CoV-2 receptor, angiotensin converting
61 enzyme 2 (ACE2). N501Y has subsequently been found in other VOCs circulating around the world,
62 i.e., B.1.351 and B.1.1.28.1 (P.1) (Coutinho et al., 2021; Lauring and Hodcroft, 2021; Tegally et al.,
63 2021a).

64 Since its first identification, SARS-CoV-2 B.1.1.7 has undergone extensive characterization. Current
65 consensus indicates that this VOC has a transmission advantage in the community (Davies et al., 2021;
66 Volz et al., 2021), possibly accompanied by increased disease severity (Challen et al., 2021), but it does
67 not appear to evade immune surveillance by natural immunity or vaccination. One hypothesis is that
68 the B.1.1.7 variant acquired its extensive range of mutations in a single immunocompromised
69 individual (Rambaut et al., 2020) who then initiated a super-spreader event that gave rise to the
70 subsequent dissemination of the lineage.
71 The P681H mutation of B.1.1.7 is of note as it is part of a proteolytic cleavage site for furin and furin-
72 like proteases at the junction of the spike protein receptor-binding (S1) and fusion (S2) domains
73 (Jaimes et al., 2020a). The S1/S2 junction of the SARS-CoV-2 S gene has a distinct indel compared to
74 all other SARS-like viruses (*Sarbecoviruses* in *Betacoronavirus* lineage B) the amino acid sequence of SARS-
75 CoV-2 S protein is $_{681}$-P-R-R-A-R|S-$_{686}$ with proteolytic cleavage (|) predicted to occur between the
76 arginine and serine residues depicted. Based on nomenclature established for proteolytic events
77 (Polgár, 1989), the R|S residues are defined as the P1|P1' residues for enzymatic cleavage, with 681H
78 of B.1.1.7 S being the P5 cleavage position. The ubiquitously-expressed serine protease furin is highly
79 specific and cleaves at a distinct multi-basic motif containing paired arginine (R) residues; furin
80 requires a minimal motif of **R**-X-X-**R** (P4-X-X-P1), with a preference for an additional basic residue
81 (histidine – H or lysine – K) at P2; i.e., **R**-X-**K/H**-**R** (Seidah and Prat, 2012). For SARS-CoV-2, the
82 presence of the S1/S2 "furin site" enhances virus transmissibility (Johnson et al., 2021; Peacock et al.,
83 2020). For B.1.1.7 S, P681H (P5) may provide an additional basic residue (especially at low pH) and
84 modulate S1/S2 cleavability by furin, and hence virus infection properties.
85 We previously studied the role of proteolytic activation of the spike protein of the prototype lineage
86 B SARS-CoV-2 (isolate Wuhan-Hu-1) (Tang et al., 2021). Here, we used a similar approach to study

87 the role of the proteolytic activation of the spike protein in the context of the B.1.1.7 VOC, with a
88 focus on the P681H point mutant.
89
90 **Results**
91 **Bioinformatic and biochemical analysis of the SARS-CoV-2 B.1.1.7 S1/S2 cleavage site**
92 To gain insight into proteolytic processing at the S1/S2 site of the B.1.1.7 spike protein, we first took
93 a bioinformatic approach utilizing the PiTou (Tian et al., 2012) and ProP (Duckert et al., 2004)
94 cleavage prediction tools, comparing B.1.1.7 to the prototype virus Wuhan-Hu-1 as well as to SARS-
95 CoV, MERS-CoV, and selected other human respiratory betacoronaviruses (HCoV-HKU1 and
96 HCoV-OC43) (Figure 1A). Both algorithms predicted a limited increase in the furin cleavage for
97 B.1.1.7 compared to Wuhan-Hu-1; in comparison SARS-CoV is not predicted to be furin-cleaved; as
98 expected, MERS-CoV showed a relatively low furin cleavage score with HCoV-HKU1 and HCoV-
99 OC43 showing much higher furin cleavage scores. Previously, we showed that the SARS-CoV-2 S1/S2
100 cleavage site is predicted to fold as a flexible loop exposed from the spike structure (Jaimes et al.,
101 2020a). Considering that the P681H mutation was predicted to slightly increase the furin cleavage at
102 this site, we modeled the SARS-CoV-2 B.1.1.7 variant spike and observed no marked changes in the
103 predicted folding, compared to Wuhan-Hu-1 (Figure 1B).
104 To directly address the activity of furin on the SARS-CoV-2 B.1.1.7 S1/S2 site, we used a biochemical
105 peptide cleavage assay (Jaimes et al., 2019). The specific peptide sequences used here were
106 TNSHRRARSVA (B.1.1.7 S1/S2) and TNSPRRARSVA (Wuhan-Hu-1 S1/S2). We tested furin, along
107 with trypsin as a control as described previously (Jaimes et al., 2020b). We also assessed the effect of
108 lowered pH because of the known properties of histidine (H) to have an ionizable side chain with a
109 p*K*a near neutrality (Nelson and Cox, 2000) (Figure 2A). As predicted, furin effectively cleaved
110 Wuhan-Hu-1 (WT) S1/S2, with B.1.1.7 S1/S2 showing a slight increase in cleavage at pH 7.5. At pH

111 7.0 and pH 6.5, B.1.1.7 S1/S2 was actually less efficiently cleaved than WT, with cleavage not
112 measurable below pH 6.5 (data not shown). Trypsin cleaved both peptides, but was less efficient than
113 furin (at pH 7.4). This comparative data with SARS-CoV S1/S2 sites reveals that the acquisition of
114 the 681H mutation does not significantly increase cleavability by furin and may in fact be inhibitory at
115 lowered pH.
116 To better understand the role of the P681H mutation in the maturation and activation of the spike
117 protein, we evaluated the expression and cleavage of the SARS-CoV-2 Wuhan-Hu-1 spike protein
118 (WT), along with the B.1.1.7 and a P681H point mutant of Wuhan-Hu-1 spikes via western blot and
119 densitometry. To do this, we used pseudoparticles consisting of a murine leukemia virus (MLV) core
120 displaying the heterologous viral envelope protein. The pseudoparticles were produced under the
121 normal furin conditions or under the presence of the protease inhibitor decanoyl-RVKR-CMK (dec-
122 RVKR-CMK) to produce cleaved and uncleaved S proteins (respectively). The purified
123 pseudoparticles were later incubated with or without furin, to better assess furin cleavage. As observed
124 in Figure 2B, partial to full cleavage was observed in all the spikes under normal cellular furin
125 conditions (no dec-RVKR-CMK nor exogenous furin), as well as in furin incubated particles.
126 Interestingly, the addition of the dec-RVKR-CMK inhibitor resulted in almost 100% uncleaved spike
127 in WT, but partially cleaved spikes in B.1.1.7 and the P681R mutant. This was also observed when
128 these particles were incubated with exogenous furin, suggesting that the P681H mutation may increase
129 furin cleavage in the complete spike. We then calculated the cleaved S vs. uncleaved S ratio for all
130 these spikes. These data were normalized to the expression of the MLV p30 protein, which is part of
131 the MLV pseudoparticles (Figure 2B). In light of the peptide cleavage data from Figure 2A, it is unclear
132 if this increased cleavage is mediated by furin or another cellular protease, possibly another member
133 of the proprotein convertase (PC) family, of which furin is a member (furin is also defined as
134 *PCSK3*/PC3) (Garten, 2018).

135

136 **Functional analysis of virus entry using viral pseudoparticles**

137 To assess the functional importance of the S1/S2 site for SARS-CoV-2 entry, we utilized the MLV
138 pseudoparticles harboring specific SARS-CoV-2 spike proteins. Particles also contain a luciferase
139 reporter that integrates into the host cell genome to drive expression of luciferase, which is quantifiable
140 (Millet et al., 2019). In this study, MLV pseudoparticles containing the SARS-CoV-2 spikes of Wuhan-
141 Hu-1 WT, B.1.1.7, and a P681H point mutant of Wuhan-Hu-1 were also generated alongside positive
142 control particles containing the vesicular stomatitis virus (VSV) G protein, and negative control
143 particles (Δ-Envelope) lacking envelope proteins (not shown), using the HEK293T cell line for
144 particle production.

145 We examined infection of SARS-CoV-2 pseudoparticles in cell lines representative of both the "early"
146 and "late" cell entry pathways (Figure 2C) as the entry mechanisms of SARS-CoV-2 can be highly cell-
147 type dependent (Whittaker et al., 2021). In this study, we utilized the Vero-TMPRSS2 ("early
148 pathway") and the Vero-E6 ("late pathway") cell lines, which are predicted to activate the SARS-CoV-
149 2 S2' using TMPRSS2 and cathepsin L respectively. While Vero-TMPRSS2 cells gave overall higher
150 luciferase signal indicative of more efficient entry, we observed little difference in infection between
151 pseudoparticles displaying spike protein from either WT, B.1.1.7 or a P681H point mutant. As
152 expected, VSVpp (positive control) infected both cell lines with several orders of magnitude higher
153 luciferase units than the values reported with Δ-Envelope infection (negative control).

154

155 **Viral growth in cell culture**

156 According to our results, the P681H mutation did not provide any molecular, nor functional advantage
157 for the B.1.1.7 variant entry into the host cell. However, we wanted to evaluate if the mutations in the
158 B.1.1.7 variant will impact the viral replication of a viral isolate in cell culture (*ex vivo*). To do this, we

159 infected Vero E6 and Vero- TMPRSS2 cells with SARS-CoV-2 strain USA-WA1/2020 or a B.1.1.7
160 isolate and evaluated the viral growth at 6-, 12-, 24- and 48-hours post-infection (p.i.) through $TCID_{50}$
161 and immunofluorescence (IFA) assays. We observed that the viral growth of the B.1.1.7 variant was
162 initially slower at 12- and 24-hours p.i., in Vero E6 cells, but it was equivalent to the USA-WA1/2020
163 growth at 48-hours p.i. (Figure 3A and 3B – Vero E6 cells panels). B.1.1.7 growth in Vero-TMPRSS2
164 cells was similar to USA-WA1/2020 during the full course of the 48-hours experiment (Figure 3A and
165 3B – Vero-TMPRSS2 panels). These results agree with our *in vitro* and functional assays, suggesting
166 that the B.1.1.7 variant does not possess a replication advantage to the USA-WA1/2020 strain *ex vivo*
167 in Vero-derived cell lines representative of both the "early" and "late" entry pathways
168
169 **Functional analysis of membrane fusion activity**
170 It has been previously reported that the B.1.1.7 variant possess an advantage in terms of transmission
171 between infected and susceptible individuals (Davies et al., 2021). However, to date, our data does not
172 show functional nor replication features in the B.1.1.7 that support any change in the viral behavior
173 and pathogenesis. Thus, we wanted to explore more directly the fusion capability of the B.1.1.7 spike
174 protein in order to see if the P681H mutation provided any advantage for cell-to-cell transmission. To
175 study this, we performed a cell-to-cell fusion assay where Vero-TMPRSS2 and VeroE6 cells were
176 transfected with the WT, B.1.1.7 and Wuhan-Hu-1 P681H spike gene and we then evaluated syncytia
177 formation as a read-out of membrane fusion (Figure 4A). While Vero-TMPRSS2 cells formed more
178 extensive syncytia than VeroE6 cells, we observed only slight differences in the syncytia formation
179 following spike protein expression for either WT, B.1.1.7, or Wuhan-Hu-1 P681H (Figure 4B). These
180 data show that the P681H mutation had little effect on membrane fusion activity of the SARS-CoV-
181 2 spike protein under the conditions tested.
182

183 **SARS-CoV-2 B.1.1.7 variant infection in human respiratory tract-derived cells**

184 So far, all our results have shown no differences between B.1.1.7 and WT behavior from molecular
185 and functional points of view. However, the functional studies were performed using susceptible cells
186 that do not necessarily represent the typical cell type that the virus will initially infect *in vivo*, which are
187 principally respiratory tract cells. To address this, we performed functional viral entry studies and live
188 virus infection assays in respiratory-type Calu-3 cells. We used the MLV pseudoparticles harboring the
189 WT, B.1.1.7 and mutated P681H spike proteins and infected Calu-3 cells. We observed slight but
190 significant differences in the luciferase transduction between WT and B.1.1.7 spike-carrying
191 pseudoparticles (Figure 5A), but no differences with the P681H mutated spike-carrying particles.,
192 compared to WT. Interestingly, we did not observe any differences in the viral growth between USA-
193 WA1/2020 and a B.1.1.7 virus isolate in Calu-3 cells (Figure 5B), which suggests that, as with Vero
194 E6 and Vero-TMPRSS2 cells, there no functional advantage for B.1.1.7 in respiratory epithelial cells;
195 i.e. Calu-3 cells.

196

197 **Discussion**

198 The factors influencing increased transmissibility and pathogenicity of SARS-CoV-2 variants remain
199 poorly understood. Here, we performed *in vitro* assays using fluorogenic peptides mimicking the S1/S2
200 sequence from both Wuhan-Hu-1 and the B.1.1.7 VOC and observed no definitive difference in furin
201 cleavage for B.1.1.7. We performed functional assays using pseudo-typed particles harboring SARS-
202 CoV-2 spike proteins and observed no significant transduction differences between Wuhan-Hu-1 and
203 B.1.1.7 spike-carrying pseudo-typed particles in VeroE6 or Vero-TMPRSS2 cells, despite the spikes
204 containing P681H being more efficiently cleaved. Likewise, we show no differences in cell-cell fusion
205 assays using the spike P681H-expressing cells, as well as no notable effects on viral replication. Our
206 findings suggest that the introduction of P681H in the B.1.1.7 variant may increase spike cleavage by

207 furin-like proteases, but this does not significantly impact viral entry, infection or cell-cell spread. We
208 consider that other factors are at play to account for the increased in transmission and disease severity
209 attributed to the SARS-CoV-2 B.1.1.7 VOC.

210 Overall, we show that the P681H mutation at the S1/S2 site of the SARS-CoV-2 spike protein may
211 increase its cleavability by furin-like proteases, but that this does not translate into increased virus
212 entry or membrane fusion. These findings are broadly in line with those of Brown *et al.* (Brown et al.,
213 2021) using infectious SARS-CoV-2, who showed no differences in the B.1.1.7 variant in terms of
214 viral replication in primary human airway cells but did show a disadvantage in Vero cells linked to
215 increased cleavage of the spike protein. In contrast, Dicken *et al.* (Dicken et al., 2021) indicated
216 enhanced entry of B.1.1.7, but in this case only under conditions with low expression of the ACE2
217 receptor.

218 B.1.1.7 is certainly not the only SARS-CoV-2 variant with a P681H change in the spike protein; it is
219 also present in B.1.243 (clade 20A), B.1.222 (clade 20B) and a lineage B.1 variant termed clade 20C,
220 with these three variants recently reported in New York State, USA (Lasek-Nesselquist et al., 2021).
221 Interestingly, B.1.243 comprised the majority of P681H-containing viruses and was the predominant
222 variant in New York in November 2020, but had declined significantly by February 2021 (to be
223 replaced by B.1.1.7 and B.1.222 among other variants) some of which do not contain P681H (e.g.,
224 B.1.429). Other examples of variants containing P681H include A.VOI.V2 detected through travel
225 surveillance in Angola, Africa (de Oliveira et al., 2021), isolates from Hawaii (Maison et al., 2021) and
226 viruses originally classified under lineage B.1.1.28 in locations such as the Philippines (Tablizo et al.,
227 2021). However, many other VOIs e.g., CAL.20C (Zhang et al., 2021) do not contain P681H. Other
228 variants containing mutations have been identified that have been proposed to impact S1/S2 cleavage,
229 e.g., A688V (Tegally et al., 2021b), but we consider such mutations to be too distal to the cleavage site
230 to have a direct impact on furin activity.

231 The SARS-CoV-2 S1/S2 site contains three basic residues in atypical spacing for a furin cleavage site
232 (Tang et al., 2021), and as such is not "polybasic". The P681H mutation increases the number of basic
233 residues to four (especially at lowered pH) and is predicted to result in a slightly increased cleavability
234 based on ProP and Pitou scoring and peptide cleavage assays at pH 7.4 (Figure 1A). However, it is
235 important to note that the P681H change does not result in the formation of a consensus furin
236 cleavage site (i.e., ^{P4}**R**-X-**K/R**-**R**^{P1}), even at lowered pH. It is also of note that increased spike protein
237 cleavage does not always translate into increased function and may in fact be detrimental. A good
238 example of this is the insertion of furin cleavage sites into SARS-CoV-1 spike at S1/S2 and/or S2',
239 which resulted in a hyper-fusogenic phenotype (Belouzard et al., 2009; Follis et al., 2006), but with
240 pseudoparticles being unrecoverable especially when added at S2' presumably due to the presence of
241 an unstable spike protein. One interpretation of the appearance of the P681H mutation in circulating
242 viruses is that SARS-CoV-2 is evolving to become a transmissible but relatively benign community-
243 acquired respiratory (CAR) or "common cold" coronavirus (Jin et al., 2020), such as the
244 betacoronaviruses HCoV-HKU1 and HCoV-OC43 both of which have very strong "polybasic" furin
245 cleavage sites at the S1/S2 position (Figure 1A). It remains to be determined how any increased
246 cleavage of SARS-CoV-2 S may affect factors such as increased duration of viral shedding, which is
247 one possible explanation of increased transmissibility for B.1.1.7. (Kissler et al., 2021).
248 As explained for other variants (including D614G in humans and Y453F in mink (Lauring and
249 Hodcroft, 2021), we consider that the rise of P681H-containing viruses could be due to chance, with
250 founder effects being responsible for rapid progression, or P681H may confer an advantage with
251 regards transmissibility or cell-cell spread *in vivo*. Our data here reinforce the concept that while analysis
252 of individual point mutations is critical part of understanding virus biology, a full assessment of the
253 epidemiological context of virus infection requires more extensive study (Goodman and Whittaker,
254 2021). It will continue to be important to track VOCs and other variants that may pose a threat for

255 exponential spreading. While the VOCs B.1.351 and B.1.1.28.1 (P.1) have been of high concern due
256 to immune escape (Coutinho et al., 2021; Darby and Hiscox, 2021; Garcia-Beltran et al., 2021; Sabino
257 et al., 2021; Tegally et al., 2020), B.1.1.7 was not considered a concern in this regard (Planas et al.,
258 2021); however, the possible acquisition of "immune-escape" mutations such as E484K or N439K
259 (Chan et al., 2020; Di Caro et al., 2021) remains possible. While B.1.1.7 remains in circulation,
260 B.1.617.2 is now outcompeting this and other variants. The three notable B.1.617 variants B.1.617.1,
261 B.1.617.2 (Delta) and B.1.617.3, along with prior variants such as A.23.1 all contain a distinct change
262 in the P5 position of the S1/S2 cleavage site (P681R), with early indications suggesting a growth
263 advantage over P681H (Peacock et al., 2021; Saito et al., 2021), possibly with the replacement of the
264 histidine in B.1.1.7 with a more conventional basic amino acid providing an important increase in viral
265 fitness in the pathway of pandemic progression. We have recently addressed the role of the P681R
266 mutation on the activation by furin, and found that the introduction of an arginine at this position,
267 could significantly increase furin activation, potentially increasing viral entry and cell-to-cell spread
268 (Lubinski et al., 2021). Other recent studies have also demonstrated that the P681R mutation enhances
269 the viral replication, and the introduction of a reverse mutation to the WT genotype P681 significantly
270 reduces the fitness of the Delta variant, to levels even lower than the Alpha variant, which harbors the
271 P681H mutation (Liu et al., 2021). These findings highlight the importance of the P681R mutation
272 and provide insights in the increased fitness of B.1.617.2/Delta.
273 B.1.1.7 remains as a VOC as defined by the World Health Organization, and has recently been moved
274 to a "variant being monitored" (VBM) as defined by the US Centers for Disease Control (CDC).
275 Despite the current global dominance of B.1.617.2/Delta (containing P618R), other P681H-
276 containing variants such as B.1.620 (Dudas et al., 2021) contain an even higher level of spike mutations
277 than B.1.1.7 (11 in total, including P681H) and are expanding in certain regions of Europe and Africa,

278 which means that the evolution of SARS-CoV-2 remains on ongoing process that needs to be carefully
279 assessed.
280
281 **Limitations of the study**
282 Bioinformatic and *in silico* analysis are predictive and they may not be fully accurate. These tools provided the
283 bases for the subsequent experiments, but they do not provide definite data. We used fluorogenic peptides
284 mimicking the SARS-CoV-2 S1/S2 regions, to evaluate the cleavage by furin and trypsin proteases. These short-
285 length peptides do not resemble the original structural folding in the native protein, and this could result in an
286 altered cleavage by the protease. Experiments using purified full-length protein may be needed to further
287 evaluate the protease cleavage. The pseudoparticle system we used for the viral entry functional experiments,
288 has been broadly described and used in previous studies by our group and other researchers globally. This
289 system provides a safe tool to study high pathogenic viruses under biosecurity level 2 (BSL-2) conditions, as
290 the pseudoparticles can mimic the viral entry but their replication is impaired, which eliminates the biosafety
291 risks. While lentivirus based pseudoparticles (like the MLV used by us) are commonly used to study
292 coronaviruses, these systems have the disadvantage that their assembly and viral envelope protein incorporation
293 differs from the normal pathways used by coronaviruses. This may affect the amount of viral envelope protein
294 that is incorporated to the pseudoparticles and hindering the evaluation of the viral infection. We performed
295 live virus infection assays to corroborate our pseudoparticle data, and observed a similar behavior, which
296 suggests that the pseudoparticle system is accurate and valid, despite differential membrane envelope protein
297 incorporation between MLV and coronaviruses.
298
299
300
301

Acknowledgements

This work was funded by the National Institute of Health research grant R01AI35270. TT is supported by the National Science Foundation Graduate Research Fellowship Program under Grant No. DGE-1650441 and the Samuel C. Fleming Family Graduate Fellowship. We would especially like to thank Hector Aguilar-Carreno and Ruth Collins for important insight, and all members of the Daniel, Diel and Whittaker groups for helpful discussions.

Author contributions

Conceptualization: B.L., T.T., S.D., J.A.J. and G.R.W.; Methodology: B.L., M.H.V.F., T.T., S.D., D.D., J.A.J. and G.R.W; Investigation: B.L., M.H.V.F., T.T., J.A.J.; Writing - Original Draft: B.L., T.T., J.A.J. and G.R.W; Writing - Review & Editing, B.L., M.H.V.F., T.T., S.D., D.D., J.A.J. and G.R.W; Visualization: B.L., M.H.V.F., T.T. and J.A.J.; Supervision: S.D., D.D., J.A.J. and G.R.W.; Funding acquisition: S.D. and G.R.W.

Declaration of Interests

The authors manifest no conflict of interest.

319 **References**

320 Belouzard, S., Chu, V.C., and Whittaker, G.R. (2009). Activation of the SARS coronavirus spike
321 protein via sequential proteolytic cleavage at two distinct sites. Proceedings of the National Academy
322 of Sciences *106*, 5871-5876.

323 Brown, J.C., Goldhill, D.H., Zhou, J., Peacock, T.P., Frise, R., Goonawardane, N., Baillon, L.,
324 Kugathasan, R., Pinto, A.L., McKay, P.F.*, et al.* (2021). Increased transmission of SARS-CoV-2
325 lineage B.1.1.7 (VOC 2020212/01) is not accounted for by a replicative advantage in primary airway
326 cells or antibody escape. bioRxiv, 2021.2002.2024.432576.

327 Challen, R., Brooks-Pollock, E., Read, J.M., Dyson, L., Tsaneva-Atanasova, K., and Danon, L.
328 (2021). Risk of mortality in patients infected with SARS-CoV-2 variant of concern 202012/1:
329 matched cohort study. BMJ *372*, n579.

330 Chan, J.F., Yuan, S., Kok, K.H., To, K.K., Chu, H., Yang, J., Xing, F., Liu, J., Yip, C.C., Poon, R.W.*,*
331 *et al.* (2020). A familial cluster of pneumonia associated with the 2019 novel coronavirus indicating
332 person-to-person transmission: a study of a family cluster. Lancet *395*, 514-523.

333 Coutinho, R.M., Marquitti, F.M.D., Ferreira, L.S., Borges, M.E., Paixão da Silva, R.L., Canton, O.,
334 Portella, T.P., Poloni, S., Franco, C., Plucinski, M.M.*, et al.* (2021). Model-based estimation of
335 transmissibility and reinfection of SARS-CoV-2 P.1 variant. medRxiv, 2021.2003.2003.21252706.

336 Darby, A.C., and Hiscox, J.A. (2021). Covid-19: variants and vaccination. BMJ *372*, n771.

337 Davies, N.G., Abbott, S., Barnard, R.C., Jarvis, C.I., Kucharski, A.J., Munday, J.D., Pearson, C.A.B.,
338 Russell, T.W., Tully, D.C., Washburne, A.D.*, et al.* (2021). Estimated transmissibility and impact of
339 SARS-CoV-2 lineage B.1.1.7 in England. Science (New York, NY) *372*, eabg3055.

340 de Oliveira, T., Lutucuta, S., Nkengasong, J., Morais, J., Paixão, J.P., Neto, Z., Afonso, P., Miranda,
341 J., David, K., Inglês, L.*, et al.* (2021). A novel variant of interest of SARS-CoV-2 with multiple spike
342 mutations detected through travel surveillance in Africa. medRxiv, 2021.2003.2030.21254323.

343 Di Caro, A., Cunha, F., Petrosillo, N., Beeching, N.J., Ergonul, O., Petersen, E., and Koopmans,
344 M.P.G. (2021). Severe acute respiratory syndrome coronavirus 2 escape mutants and protective
345 immunity from natural infections or immunizations. Clinical Microbiology and Infection *27*, 823-
346 826.

347 Dicken, S.J., Murray, M.J., Thorne, L.G., Reuschl, A.-K., Forrest, C., Ganeshalingham, M., Muir, L.,
348 Kalemera, M.D., Palor, M., McCoy, L.E.*, et al.* (2021). Characterisation of B.1.1.7 and Pangolin
349 coronavirus spike provides insights on the evolutionary trajectory of SARS-CoV-2. bioRxiv,
350 2021.2003.2022.436468.

351 Duckert, P., Brunak, S., and Blom, N. (2004). Prediction of proprotein convertase cleavage sites.
352 Protein Engineering, Design and Selection *17*, 107-112.

353 Dudas, G., Hong, S.L., Potter, B., Calvignac-Spencer, S., Niatou-Singa, F.S., Tombolomako, T.B.,
354 Fuh-Neba, T., Vickos, U., Ulrich, M., Leendertz, F.H.*, et al.* (2021). Travel-driven emergence and
355 spread of SARS-CoV-2 lineage B.1.620 with multiple VOC-like mutations and deletions in Europe.
356 medRxiv, 2021.2005.2004.21256637.

357 Follis, K.E., York, J., and Nunberg, J.H. (2006). Furin cleavage of the SARS coronavirus spike
358 glycoprotein enhances cell–cell fusion but does not affect virion entry. Virology *350*, 358-369.

359 Garcia-Beltran, W.F., Lam, E.C., St. Denis, K., Nitido, A.D., Garcia, Z.H., Hauser, B.M., Feldman,
360 J., Pavlovic, M.N., Gregory, D.J., Poznansky, M.C., *et al.* (2021). Multiple SARS-CoV-2 variants
361 escape neutralization by vaccine-induced humoral immunity. Cell *184*, 2372-2383.e2379.

362 Garten, W. (2018). Characterization of Proprotein Convertases and Their Involvement in Virus
363 Propagation. Activation of Viruses by Host Proteases, 205-248.

364 Goodman, L.B., and Whittaker, G.R. (2021). Public health surveillance of infectious diseases:
365 beyond point mutations. The Lancet Microbe *2*, e53-e54.

366 Jaimes, J.A., Andre, N.M., Chappie, J.S., Millet, J.K., and Whittaker, G.R. (2020a). Phylogenetic
367 Analysis and Structural Modeling of SARS-CoV-2 Spike Protein Reveals an Evolutionary Distinct
368 and Proteolytically Sensitive Activation Loop. Journal of molecular biology.

369 Jaimes, J.A., Millet, J.K., Goldstein, M.E., Whittaker, G.R., and Straus, M.R. (2019). A Fluorogenic
370 Peptide Cleavage Assay to Screen for Proteolytic Activity: Applications for coronavirus spike protein
371 activation. J Vis Exp.

372 Jaimes, J.A., Millet, J.K., and Whittaker, G.R. (2020b). Proteolytic Cleavage of the SARS-CoV-2
373 Spike Protein and the Role of the Novel S1/S2 Site. iScience *23*.

374 Jin, X., Xu, K., Jiang, P., Lian, J., Hao, S., Yao, H., Jia, H., Zhang, Y., Zheng, L., Zheng, N., *et al.*
375 (2020). Virus strain from a mild COVID-19 patient in Hangzhou represents a new trend in SARS-
376 CoV-2 evolution potentially related to Furin cleavage site. Emerging microbes & infections *9*, 1474-
377 1488.

378 Johnson, B.A., Xie, X., Bailey, A.L., Kalveram, B., Lokugamage, K.G., Muruato, A., Zou, J., Zhang,
379 X., Juelich, T., Smith, J.K., *et al.* (2021). Loss of furin cleavage site attenuates SARS-CoV-2
380 pathogenesis. Nature *591*, 293-299.

381 Kissler, S.M., Fauver, J.R., Mack, C., Tai, C.G., Breban, M.I., Watkins, A.E., Samant, R.M.,
382 Anderson, D.J., Ho, D.D., Metti, J., *et al.* (2021). Densely sampled viral trajectories for SARS-CoV-2
383 variants alpha (B.1.1.7) and epsilon (B.1.429). medRxiv, 2021.2002.2016.21251535.

384 Lasek-Nesselquist, E., Pata, J., Schneider, E., and George, K.S. (2021). A tale of three SARS-CoV-2
385 variants with independently acquired P681H mutations in New York State. medRxiv,
386 2021.2003.2010.21253285.

387 Lauring, A.S., and Hodcroft, E.B. (2021). Genetic Variants of SARS-CoV-2—What Do They Mean?
388 JAMA *325*, 529-531.

389 Liu, Y., Liu, J., Johnson, B.A., Xia, H., Ku, Z., Schindewolf, C., Widen, S.G., An, Z., Weaver, S.C.,
390 Menachery, V.D., *et al.* (2021). Delta spike P681R mutation enhances SARS-CoV-2 fitness over
391 Alpha variant. bioRxiv, 2021.2008.2012.456173.

392 Lubinski, B., Frazier, L.E., Phan, M.V.T., Bugembe, D.L., Tang, T., Daniel, S., Cotten, M., Jaimes,
393 J.A., and Whittaker, G.R. (2021). Spike protein cleavage-activation mediated by the SARS-CoV-2
394 P681R mutation: a case-study from its first appearance in variant of interest (VOI) A.23.1 identified
395 in Uganda. bioRxiv, 2021.2006.2030.450632.

396 Maison, D.P., Ching, L.L., Shikuma, C.M., and Nerurkar, V.R. (2021). Genetic Characteristics and
397 Phylogeny of 969-bp S Gene Sequence of SARS-CoV-2 from Hawaii Reveals the Worldwide
398 Emerging P681H Mutation. bioRxiv, 2021.2001.2006.425497.

399 Millet, J.K., Tang, T., Nathan, L., Jaimes, J.A., Hsu, H.L., Daniel, S., and Whittaker, G.R. (2019).
400 Production of Pseudotyped Particles to Study Highly Pathogenic Coronaviruses in a Biosafety Level
401 2 Setting. J Vis Exp.

402 Nelson, D.L., and Cox, M.M. (2000). Lehninger Principles of Biochemistry (Worth Publishers).

403 Peacock, T.P., Goldhill, D.H., Zhou, J., Baillon, L., Frise, R., Swann, O.C., Kugathasan, R., Penn, R.,
404 Brown, J.C., Sanchez-David, R.Y., *et al.* (2020). The furin cleavage site of SARS-CoV-2 spike protein
405 is a key determinant for transmission due to enhanced replication in airway cells. bioRxiv,
406 2020.2009.2030.318311.

407 Peacock, T.P., Sheppard, C.M., Brown, J.C., Goonawardane, N., Zhou, J., Whiteley, M., de Silva,
408 T.I., and Barclay, W.S. (2021). The SARS-CoV-2 variants associated with infections in India,
409 B.1.617, show enhanced spike cleavage by furin. bioRxiv, 2021.2005.2028.446163.

410 Planas, D., Bruel, T., Grzelak, L., Guivel-Benhassine, F., Staropoli, I., Porrot, F., Planchais, C.,
411 Buchrieser, J., Rajah, M.M., Bishop, E., *et al.* (2021). Sensitivity of infectious SARS-CoV-2 B.1.1.7
412 and B.1.351 variants to neutralizing antibodies. Nature Medicine *27*, 917-924.

413 Polgár, L. (1989). General Aspects of Proteases. In Mechanisms of Protease Action (Boca Raton,
414 FL: CRC press), pp. 43-86.

415 Rambaut, A., Loman, N., Pybus, O., Barclay, W., Barrett, J., Carabelli, A., Connor, T., Peacock, T.,
416 Robertson, D.L., and Volz, E. (2020). Preliminary genomic characterisation of an emergent SARS-
417 CoV-2 lineage in the UK defined by a novel set of spike mutations (Virological).

418 Sabino, E.C., Buss, L.F., Carvalho, M.P.S., Prete, C.A., Crispim, M.A.E., Fraiji, N.A., Pereira,
419 R.H.M., Parag, K.V., da Silva Peixoto, P., Kraemer, M.U.G., *et al.* (2021). Resurgence of COVID-19
420 in Manaus, Brazil, despite high seroprevalence. The Lancet *397*, 452-455.

421 Saito, A., Nasser, H., Uriu, K., Kosugi, Y., Irie, T., Shirakawa, K., Sadamasu, K., Kimura, I., Ito, J.,
422 Wu, J., *et al.* (2021). SARS-CoV-2 spike P681R mutation enhances and accelerates viral fusion.
423 bioRxiv, 2021.2006.2017.448820.

424 Seidah, N.G., and Prat, A. (2012). The biology and therapeutic targeting of the proprotein
425 convertases. Nature Reviews Drug Discovery *11*, 367-383.

426 Tablizo, F.A., Kim, K.M., Lapid, C.M., Castro, M.J.R., Yangzon, M.S.L., Maralit, B.A., Ayes, M.E.C.,
427 Cutiongco-de la Paz, E.M., De Guzman, A.R., Yap, J.M.C., *et al.* (2021). Genome sequencing and
428 analysis of an emergent SARS-CoV-2 variant characterized by multiple spike protein mutations
429 detected from the Central Visayas Region of the Philippines. medRxiv, 2021.2003.2003.21252812.

430 Tang, T., Jaimes, J.A., Bidon, M.K., Straus, M.R., Daniel, S., and Whittaker, G.R. (2021). Proteolytic
431 Activation of SARS-CoV-2 Spike at the S1/S2 Boundary: Potential Role of Proteases beyond Furin.
432 ACS Infectious Diseases *7*, 264-272.

433 Tegally, H., Wilkinson, E., Giovanetti, M., Iranzadeh, A., Fonseca, V., Giandhari, J., Doolabh, D.,
434 Pillay, S., San, E.J., Msomi, N., *et al.* (2020). Emergence and rapid spread of a new severe acute
435 respiratory syndrome-related coronavirus 2 (SARS-CoV-2) lineage with multiple spike mutations in
436 South Africa. medRxiv, 2020.2012.2021.20248640.

437 Tegally, H., Wilkinson, E., Giovanetti, M., Iranzadeh, A., Fonseca, V., Giandhari, J., Doolabh, D.,
438 Pillay, S., San, E.J., Msomi, N., *et al.* (2021a). Detection of a SARS-CoV-2 variant of concern in
439 South Africa. Nature *592*, 438-443.

440 Tegally, H., Wilkinson, E., Lessells, R.J., Giandhari, J., Pillay, S., Msomi, N., Mlisana, K., Bhiman,
441 J.N., von Gottberg, A., Walaza, S.*, et al.* (2021b). Sixteen novel lineages of SARS-CoV-2 in South
442 Africa. Nature Medicine *27*, 440-446.

443 Tian, S., Huajun, W., and Wu, J. (2012). Computational prediction of furin cleavage sites by a hybrid
444 method and understanding mechanism underlying diseases. Sci Rep *2*, 261.

445 Volz, E., Mishra, S., Chand, M., Barrett, J.C., Johnson, R., Geidelberg, L., Hinsley, W.R., Laydon,
446 D.J., Dabrera, G., O'Toole, Á.*, et al.* (2021). Assessing transmissibility of SARS-CoV-2 lineage
447 B.1.1.7 in England. Nature *593*, 266-269.

448 Whittaker, G.R., Daniel, S., and Millet, J.K. (2021). Coronavirus entry: how we arrived at SARS-
449 CoV-2. Current Opinion in Virology *47*, 113-120.

450 Zhang, W., Davis, B.D., Chen, S.S., Sincuir Martinez, J.M., Plummer, J.T., and Vail, E. (2021).
451 Emergence of a Novel SARS-CoV-2 Variant in Southern California. JAMA *325*, 1324-1326.

452 Zhou, B., Thao, T.T.N., Hoffmann, D., Taddeo, A., Ebert, N., Labroussaa, F., Pohlmann, A., King,
453 J., Steiner, S., Kelly, J.N.*, et al.* (2021). SARS-CoV-2 spike D614G change enhances replication and
454 transmission. Nature *592*, 122-127.

455

456

457

458

459

460

461

462

463

464

465

466

467

468

469

470 **Figures and figure legends:**
471

A

Virus	S1/S2 Sequence	Furin Score PiTou	Furin Score ProP
SARS-CoV-2 (WT)	672-ASYQTQTNSPRRAR|SVASQS-691	+9.196	0.620
SARS-CoV-2 (B.1.1.7)	669-ASYQTQTNSHRRAR|SVASQS-688	+9.907	0.704
SARS-CoV	654-AGICASYHTVSLLR|STSQKS-673	–5.167	0.123
MERS-CoV	738-LPDTPSTLTPRSVR|SVPGEM-757	+5.155	0.563
HCoV-HKU1	747-YNSPSSSSSRRKRR|SISASY-766	+14.634	0.918
HCoV-OC43 (clinical)	750-GYCVDYFKNRRSRR|AITTGY-769	+10.10	0.736

B

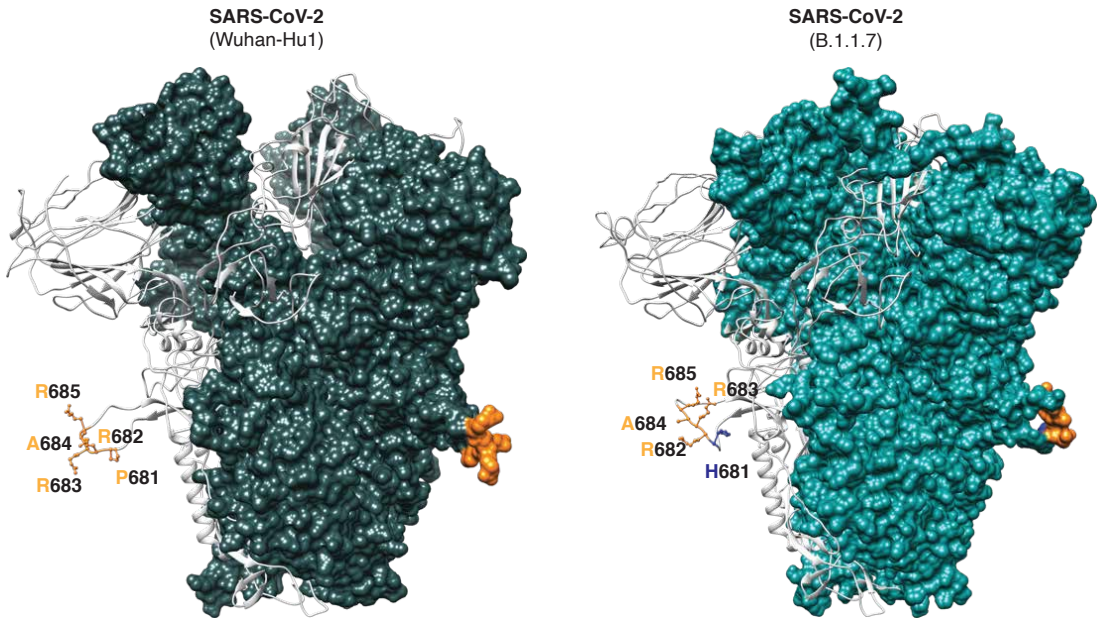

472
473
474
475 **Figure 1. SARS-CoV-2 spike S1/S2 cleavage site.**
476 **A.** Furin cleavage score analysis of CoV S1/S2 cleavage sites. CoV S sequences were analyzed using
477 the ProP 1.0 and PiTou 3.0 furin prediction algorithm, generating a score with bold numbers indicating
478 predicted furin cleavage. (|) denotes the position of the predicted S1/S2 cleavage site. Basic resides,
479 arginine (R) and lysine (K), are highlighted in blue, with histidine in purple. Sequences corresponding
480 to the S1/S2 region of SARS-CoV-2 (QHD43416.1), SARS-CoV (AAT74874.1), MERS-CoV
481 (AFS88936.1), HCoV-HKU1 (AAT98580.1), HCoV-OC43 (KY369907.1) were obtained from
482 GenBank. Sequences corresponding to the S1/S2 region of SARS-CoV-2 B.1.1.7 (EPI_ISL_1374509)
483 was obtained from GISAID. **B.** SARS-CoV-2 spike structural models. Homology models were built
484 for the spike protein from Wuhan-Hu1 (WT) and B.1.1.7 variants. The S1/S2 cleavage site sequences
485 are noted. WT sequence $_{681}$PRRAR$_{685}$ is noted in orange and mutated residue H681 is noted in blue.
486

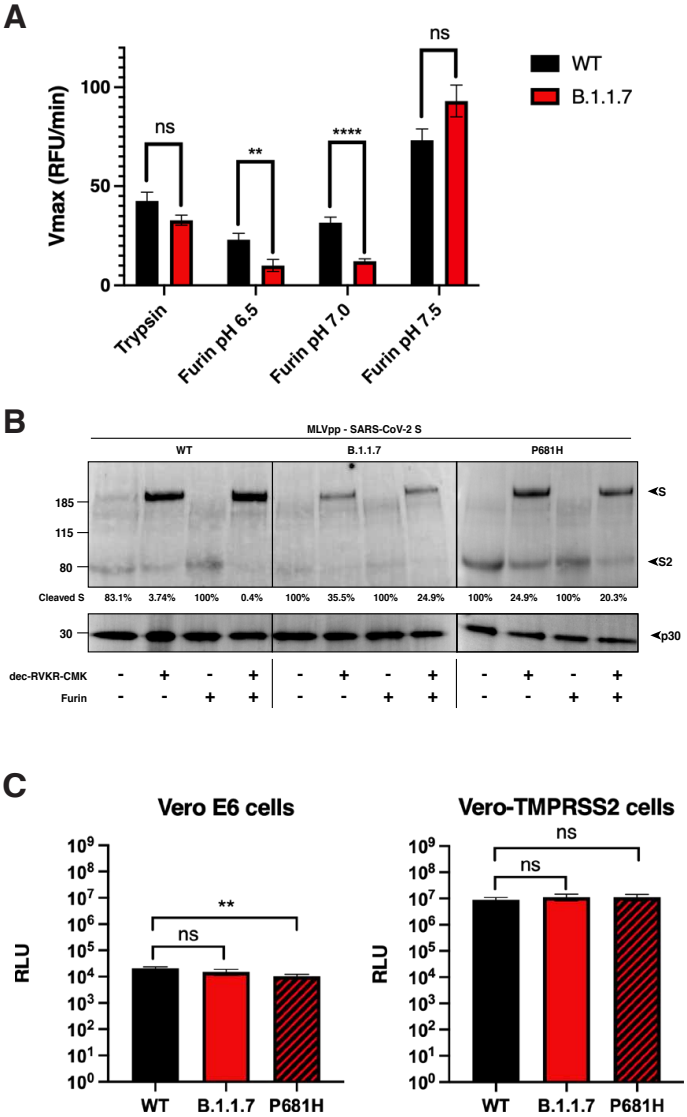

Figure 2. SARS-CoV-2 B.1.1.7 variant S1/S2 cleavage site activation and role in viral entry. **A.** Fluorogenic peptide cleavage assays of the SARS-CoV-2 S1/S2 cleavage site. Peptides mimicking the S1/S2 site of the SARS-CoV-2 WT and B.1.1.7 variants were evaluated for *in vitro* cleavage by trypsin and furin proteases at pH 7.4 (trypsin), and pH 6.5, 6.0 and 7.5 (furin) conditions. A significant decrease in the cleavage of the B.1.1.7 S1/S2 peptide by furin was observed at pH 6.5 and 7.0 compared to WT. In contrast, a non-significant increase in the furin cleavage of the B.1.1.7 peptide was observed at pH 7.5. **B.** Western blot analysis of MLV pseudoparticles (MLVpps) carrying the WT, B.1.1.7, or P681H S. Uncleaved S (~185 kDa) and cleaved S2 (~85 kDa) detection was conducted using an antibody targeting the SARS-CoV-2 S2 domain. + dec-RVKR-CMK refers to MLVpp produced in HEK-293T cells treated with 75 µM dec-RVKR-CMK at the time of transfection. + furin refers to particles treated with 6 U of recombinant furin for 3 h at 37 °C. **C.** Ratio of the intensity of cleaved S band to uncleaved S in MLV pseudoparticles. Band intensity was normalized to the uncleaved band intensity of each pseudoparticle and cleavage ratio was calculated. **D.** Pseudoparticle infectivity assays in Vero E6 and Vero-TMPRSS2 cells. Cells were infected with MLV pseudoparticles harboring the VSV-G, SARS-CoV-2 S WT, SARS-CoV-2 S B.1.1.7 variant, SARS-CoV-2 S WT with P681H mutation. Data represents the average luciferase activity of cells of four biological replicates. No significant differences in luciferase transduction were observed between the infected cells.

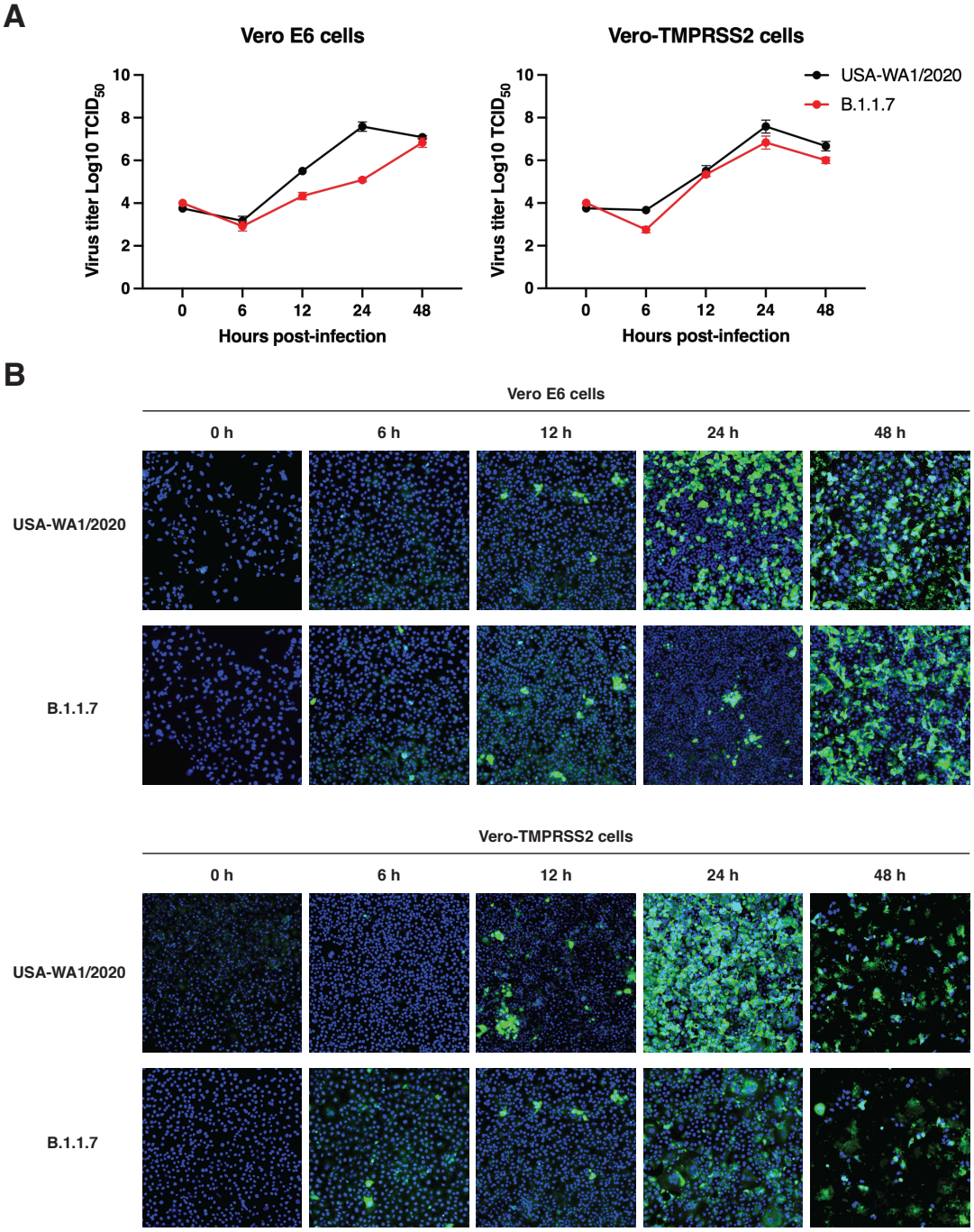

Figure 3. SARS-CoV-2 B.1.1.7 variant infectivity *ex vivo*.
A. SARS-CoV-2 WA1/2020 and B.1.1.7 growth curves on Vero E6 and Vero-TMPRSS2 cells. Cells were infected to a MOI of 0.1 and supernatant was collected at 0-, 6-, 12-, 24- and 48-hours p.i. Growth curves were then calculated using $TCID_{50}$. **B.** Immunofluorescence assay (IFA) of SARS-CoV-2 WA1/2020 and B.1.1.7 infection on Vero E6 and Vero-TMPRSS2 cells. Cells were infected to a MOI of 0.1 and IFA was performed 0, 6, 12, 24 and 48 hours p.i. Detection of infected cells (green) was conducted using an antibody targeting the SARS-CoV-2 S2 domain. Cell nuclei was stained using DAPI (blue).

516

A

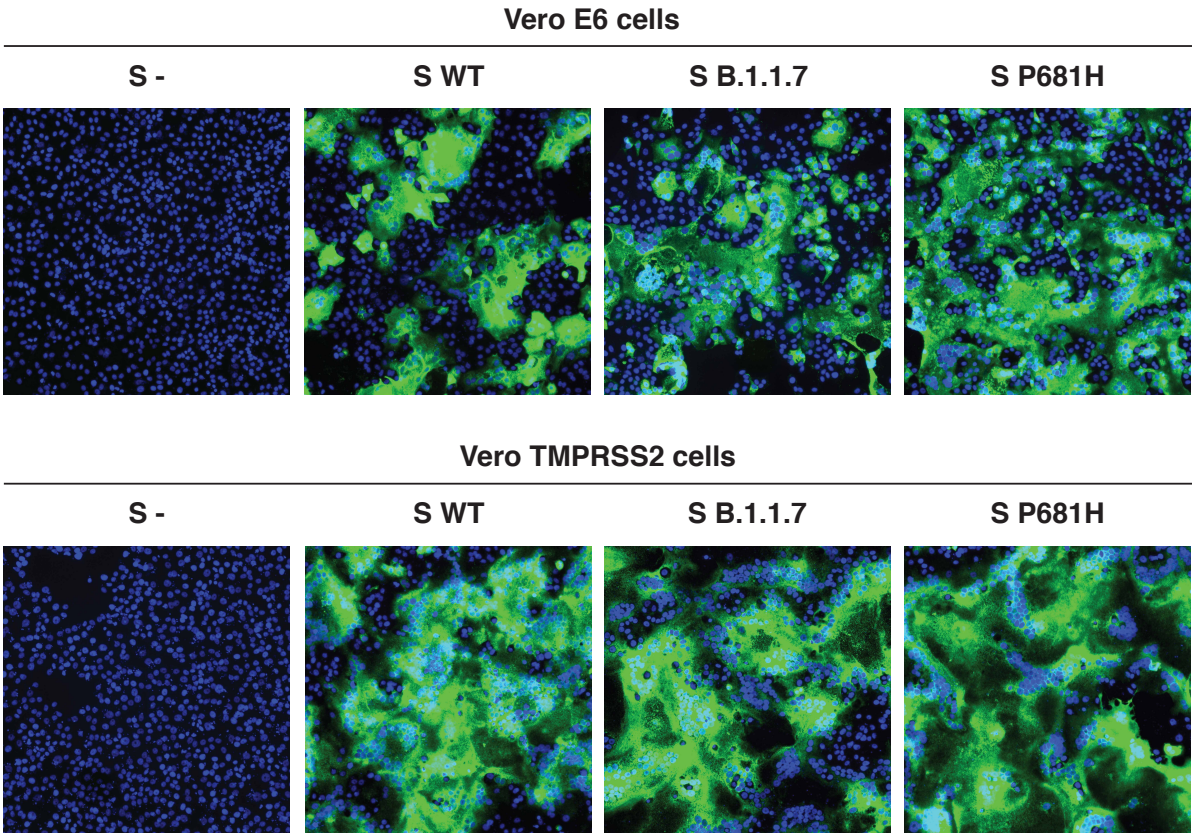

B

Vero E6 cells

	# Syncytia (cells with 4+ nuclei)	# Total nuclei	# Nuclei involved in syncytia	% Nuclei involved in syncytia
S -	0	1359	0	0
S WT	9	906	365	40.29
S B117	5	823	366	44.47
S P681H	5	940	573	60.96

Vero-TMPRSS2 cells

	# Syncytia (cells with 4+ nuclei)	# Total nuclei	# Nuclei involved in syncytia	% Nuclei involved in syncytia
S -	0	1038	0	0
S WT	1	985	793	80.51
S B117	1	918	758	82.57
S P681H	1	772	656	84.97

517
518
519 **Figure 4. Cell-to-cell fusion in SARS-CoV-2 B.1.1.7 S expressing cells**
520 **A.** Cell-to-cell fusion in Vero E6 and Vero-TMPRSS2 cells expressing SARS-CoV-2 S. Cells were
521 transfected with a plasmid carrying the WT, B.1.1.7, or P681H S gene and evaluated through IFA after
522 28 hours. Syncytia formation was observed using an antibody targeting the SARS-CoV-2 S2 domain
523 and a DAPI for cell nuclei (blue). **B.** Syncytia counting in SARS-CoV-2 S expressing cells. Total of
524 nuclei per cell were counted to determine the percentage of nuclei involved in syncytia.
525
526
527
528
529
530
531

532

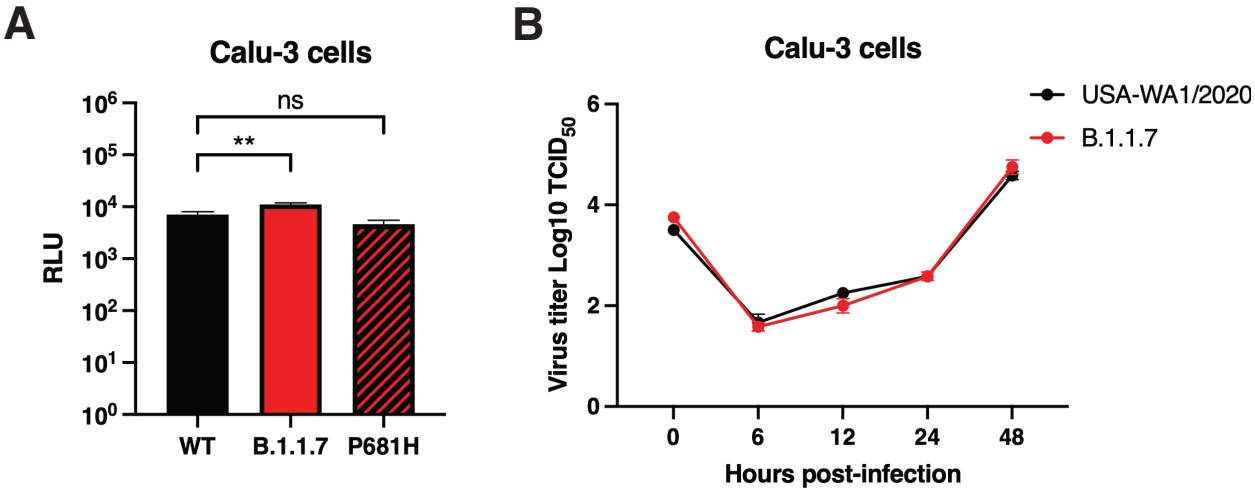

533
534
535 **Figure 5. Infection in respiratory Calu-3 cells.**
536 **A.** Pseudoparticle infectivity assays in Calu-3 cells. Cells were infected with MLV pseudoparticles
537 harboring the VSV-G, SARS-CoV-2 S WT, SARS-CoV-2 S B.1.1.7 variant, SARS-CoV-2 S WT with
538 P681H mutation. Data represents the average luciferase activity of cells of three biological replicates.
539 A significant increase in the luciferase transduction were observed with the pseudoparticles harboring
540 the B.1.1.7 S (P=0.0076). **B.** SARS-CoV-2 WA1/2020 and B.1.1.7 growth curves on Calu-3 cells. Cells
541 were infected to a MOI of 0.1 and supernatant was collected at 0-, 6-, 12-, 24- and 48-hours p.i.
542 Growth curves were then calculated using $TCID_{50}$.
543

544

545

546

547

548

549

550

551

552

553

554

555

556 **Methods**

557 **Furin prediction calculations:** Prop: CoV sequences were analyzed using the ProP 1.0 Server hosted
558 at: cbs.dtu.dk/services/ProP/. PiTou: CoV sequences were analyzed using the PiTou V3 software
559 hosted at: http://www.nuolan.net/reference.html.

560

561 ***In silico* homology modeling:** SARS-CoV-2 S protein models for Wuhan Hu-1 (GenBank accession
562 # MN908947.3) and B.1.1.7 hCoV-19/England/MILK-9E05B3/2020 (GISAID accession #
563 EPI_ISL_601443 – Original sample and sequence submission information included in table 1), were
564 built using UCSF Chimera (v.1.14, University of California) through the homology modeling tool of
565 the Modeller extension (v.10.1, University of California) as described in (Jaimes et al., 2020a). Models
566 were built based on the SARS-CoV S structure (PDB No. 5X58).

Virus Name	Accession Number	Originating Laboratory	Submitting Laboratory	Authors	Submitter
hCoV-19/England/MILK-9E05B3/2020	EPI_ISL_601443	Lighthouse Lab in Milton Keynes	Wellcome Sanger Institute for the COVID-19 Genomics UK (COG-UK) consortium	The Lighthouse Lab in Milton Keynes and Alex Alderton, Roberto Amato, Sonia Goncalves, Ewan Harrison, David K. Jackson, Ian Johnston, Dominic Kwiatkowski, Cordelia Langford, John Sillitoe on behalf of the Wellcome Sanger Institute COVID-19 Surveillance Team (http://www.sanger.ac.uk/covid-team)	Robert Davies

567 **Table 1: SARS-CoV-2 B.1.1.7 variant original sample and sequence submission information.**

568

569 **Fluorogenic peptide assays:** Fluorogenic peptide assays were performed as described previously
570 with minor modifications (Jaimes et al., 2019). Each reaction was performed in a 100 µL volume
571 consisting of buffer, protease, and SARS-CoV-2 S1/S2 WT (TNSPRRARSVA) or SARS-CoV-2
572 S1/S2 B.1.1.7 (TNSHRRARSVA) fluorogenic peptide in an opaque 96-well plate. For trypsin

573 catalyzed reactions, 0.8 nM/well TPCK trypsin was diluted in PBS buffer. For furin catalyzed
574 reactions, 1 U/well recombinant furin was diluted in buffer consisting of 20 mM HEPES, 0.2 mM
575 CaCl2, and 0.2 mM β-mercaptoethanol, at pH 6.5, 7.0 or 7.5. Fluorescence emission was measured
576 once per minute for 60 continued minutes using a SpectraMax fluorometer (Molecular Devices, Inc.)
577 at 30 °C with an excitation wavelength of 330 nm and an emission wavelength of 390 nm. Vmax was
578 calculated by fitting the linear rise in fluorescence to the equation of a line.
579
580 **Synthesis and cloning of the B.1.1.7 spike protein:** The B.1.1.7 spike gene from isolate hCoV-
581 19/England/MILK-9E05B3/2020 (EPI_ISL_601443) was codon-optimized, synthesized and cloned
582 into a pcDNA 3.1+ vector for expression (GenScript Biotech Co.).
583
584 **Site-directed mutagenesis:** Mutagenesis primers (cagacctggctctcctgtgggagtttgtctgggt/
585 acccagacaaactcccacaggagagccaggtctg) were designed based on the DNA sequence for SARS-CoV-2
586 Wuhan-Hu-1 using the QuickChange Primer Design tool (Agilent Technologies, Inc.). Mutagenesis
587 was carried out on a pCDNA-SARs2 Wuhan-Hu 1 S plasmid to create the P681H mutation, using the
588 QuickChange Lightning Mutagenesis kit (Agilent Technologies, Inc.). The original plasmid was
589 generously provided by David Veesler, University of Washington USA. XL-10 gold competent cells
590 were transformed with the mutated plasmid, plated on LB Agar + Ampicillin plates, and left at 37°C
591 overnight. A distinct colony was chosen the next day to grow up a 4 ml small culture at 37°C overnight.
592 pCDNA-SARC-CoV-2 Wuhan-Hu-1 P681H S plasmid was then extracted using the QIAprep Spin
593 Miniprep Kit (Qiagen N.V.) and Sanger sequencing was used to confirm incorporation of the
594 mutation.
595

596 **Pseudoparticle generation:** HEK-293T cells were seeded at $3x10^5$ cells/ml in a 6-well plate the day
597 before transfection. Transfection was performed using polyethylenimine (PEI) and 1X Gibco® Opti-
598 Mem (Life Technologies Co.). Cells were transfected with 800ng of pCMV-MLV *gag-pol*, 600ng of
599 pTG-Luc, and 600 ng of a plasmid containing the viral envelope protein of choice. Viral envelope
600 plasmids included pCAGGS-VSV G as a positive control, pCDNA-SARS-CoV-2 Wuhan-Hu-1 S,
601 pCDNA- SARS-CoV-2 (Wuhan-Hu-1) P681H S, and pCDNA-SARS-CoV-2 B.1.1.7 S. pCAGGS
602 empty vector was used for a Δ-Envelope negative control. 48 hours post transfection, the supernatant
603 containing the pseudoparticles was removed, centrifuged to remove cell debris, filtered, and stored at
604 -80°C. For + dec-RVKR-CMK particles, 7.5 μL of dec-RVKR-CMK was added to cells immediately
605 after transfection.
606
607 **Pseudoparticle Infection Assay:** Vero E6 and Vero-TMPRSS2 cells were seeded at $3x10^5$ cells/ml
608 in a 24 well plate the day before infection. Cells were washed three times with 1X DPBS and then
609 infected with 200 μl of either VSV G, SARS-CoV-2 S, SARS-Cov-2 P681H S, SARS-CoV-2 B.1.1.7
610 S, or Δ-Envelope pseudoparticles. Infected cells incubated on a rocker for 1.5 hours at 37°C, then 300
611 μl of complete media were added and cells were left at 37°C. At 72 hours post-infection, cells were
612 lysed and the level of infection was assessed using the Luciferase Assay System (Cat: E1501, Promega
613 Co.). The manufacturer's protocol was modified by putting the cells through 3 freeze/thaw cycles
614 after the addition of 100 μl of the lysis reagent. 10 μl of the cell lysate were added to 20 μl of luciferin,
615 and then luciferase activity was measured using the Glomax 20/20 luminometer (Promega Co.).
616 Infection assays were done in triplicate and were replicated 4 times. All four replicates were carried
617 out using pseudoparticles generated from the same transfection.
618

619 **Western blot analysis of pseudoparticles:** 3 mL of pseudoparticles were pelleted using a TLA-55
620 rotor with an Optima-MAX-E ultracentrifuge (Beckman Coulter, Inc.) for 2 hours at 42,000 rpm at
621 4°C. Untreated particles were resuspended in 30 μL DPBS buffer. For the + furin treated MLVpps,
622 particles were resuspended in 30 μL of furin buffer consistent in 20 mM HEPES, 0.2 mM CaCl2, and
623 0.2 mM β-mercaptoethanol (at pH 7.0). Particles were later incubated with 6 U of recombinant furin
624 for 3 h at 37 °C. Sodium dodecyl sulfate (SDS) loading buffer and DTT were added to samples and
625 heated at 65°C for 20 minutes. Samples were separated on NuPAGE Bis-Tris gel (Cat: NP0321BOX,
626 Invitrogen Co.) and transferred on polyvinylidene difluoride (PVDF) membranes (MilliporeSigma).
627 SARS-CoV-2 S was detected using a rabbit polyclonal antibody against the S2 domain (Cat: 40590-
628 T62, Sino Biological, Inc) and an AlexaFluor™ 488 goat anti-rabbit antibody (Invitrogen Co, USA).
629 Bands were detected using the ChemiDoc (Bio-Rad Laboratories, Inc.) and band intensity was
630 calculated using the analysis tools on Image Lab 6.1 software (Bio-Rad Laboratories, Inc.) to determine
631 the uncleaved-to-cleaved S ratios.
632
633 **Growth curves:** SARS-CoV-2 WA1/2020 and B.1.1.7 growth curves were performed in Vero E6,
634 Vero-TMPRSS2 and Calu-3 cells. Cells were cultured in 24-well plates in advance, inoculated with a
635 multiplicity of infection (MOI) of 0.1 and harvested at 6-, 12-, 24- and 48-hours post-infection (p.i.)
636 in triplicate. Virus titers were determined on each time by limiting dilutions in Vero E6 cells. At 48-
637 hours p.i. cells were fixed (3.7% formaldehyde), permeabilized (0.2% Triton-X), and stained with an
638 anti-NP SARS-CoV-2 rabbit polyclonal antibody (produced and characterized in Diel laboratory) and
639 then incubated with a goat anti-rabbit IgG secondary antibody (Alexa Fluor 594; Immunoreagents).
640 Viral titers were determined by the Spearman and Karber's method and expressed as tissue culture
641 infectious dose 50 ($TCID_{50}$) per milliliter.
642

643 **Immunofluorescence assay:** Vero E6 and Vero-TMPRSS2 cells cultured in 4-well glass slides were
644 infected with SARS-CoV-2 WA1/2020 and B.1.1.7 (MOI = 0.1). At 0-, 6-, 12-, 24- and 48-hours p.i.
645 cells were fixed using 3.7% formaldehyde in PBS (pH 7.2) for 30 min. The cells were washed three
646 times with PBS and quenched with 50 mM NH4Cl. Permeabilization was performed with 0.1% Triton
647 X-100 in PBS for 5 minutes on ice. Blocking was performed using 5% heat inactivated goat serum in
648 PBS for 20 minutes and the antibodies for labeling were diluted in the same solution. The spike
649 expression was detected using the SARS-CoV-2 spike antibody (Cat: 40591-T62, Sino Biological Inc.)
650 at 1/500 dilution for 1 hour. Secondary antibody labeling was performed using AlexaFluor™ 488 goat
651 anti-rabbit IgG antibody (Cat: A32731, Invitrogen Co.) at a 1/500 dilution for 45 minutes. Three
652 washes with PBS were performed between each step of the assay. Finally, slides were mounted using
653 DAPI Fluoromount-G® (Cat: 0100-20, SouthernBiotech Inc.) and analyzed with fluorescence.
654
655 **Cell-cell fusion assay:** Vero E6 and Vero-TMPRSS2 cells were transfected with a plasmid harboring
656 the spike gene of the SARS-CoV-2 Wuhan-Hu 1, SARS-CoV-2 B.1.1.7, the SARS-CoV-2 P681H S,
657 or a delta-spike pCDNA3.1+ plasmid, and evaluated through an immunofluorescence assay (IFA).
658 Transfection was performed on 8-well glass slides at 90% confluent cells using Lipofectamine® 3000
659 (Cat: L3000075, Invitrogen Co.), following the manufacturer's instructions and a total of 250 ng of
660 DNA per well was transfected. The cells were then incubated at 37°C with 5% of CO_2 for 28 hours.
661 Syncytia was visualized through an immunofluorescence assay using the method described in the
662 previous section. Representative images of each treatment group were taken, and these images were
663 used to calculate the percent of nuclei involved in the formation of syncytia. Images were taken at
664 20X on the Echo Revolve fluorescent microscope (Model: RVL-100-M). The nuclei were counted
665 manually using the Cell Counter plugin in ImageJ (https://imagej.nih.gov/ij/). Cells that expressed
666 the spike protein and contained 4 or more nuclei were considered to be one syncytia.